Inverted allosteric coupling between activation and inactivation gates in K^+ channels

Alain J. Labro[a], D. Marien Cortes[b,c], Cholpon Tilegenova[b,c,1], and Luis G. Cuello[b,c,2]

[a]Laboratory for Molecular, Cellular and Network Excitability, University of Antwerp, 2610 Antwerp, Belgium; [b]Cell Physiology and Molecular Biophysics, Texas Tech University Health Sciences Center, Lubbock, TX 79430; and [c]Center for Membrane Protein Research, Texas Tech University Health Sciences Center, Lubbock, TX 79430

Edited by Richard W. Aldrich, The University of Texas at Austin, Austin, TX, and approved April 17, 2018 (received for review January 10, 2018)

The selectivity filter and the activation gate in potassium channels are functionally and structurally coupled. An allosteric coupling underlies C-type inactivation coupled to activation gating in this ion-channel family (i.e., opening of the activation gate triggers the collapse of the channel's selectivity filter). We have identified the second Threonine residue within the TTVGYGD signature sequence of K^+ channels as a crucial residue for this allosteric communication. A Threonine to Alanine substitution at this position was studied in three representative members of the K^+-channel family. Interestingly, all of the mutant channels exhibited lack of C-type inactivation gating and an inversion of their allosteric coupling (i.e., closing of the activation gate collapses the channel's selectivity filter). A state-dependent crystallographic study of KcsA-T75A proves that, on activation, the selectivity filter transitions from a nonconductive and deep C-type inactivated conformation to a conductive one. Finally, we provide a crystallographic demonstration that closed-state inactivation can be achieved by the structural collapse of the channel's selectivity filter.

C-type inactivation | KcsA | allosteric coupling | Kv 1.5 | Shaker channel

Conformational changes at the pore domain (PD) of K^+ channels underlie the rapid interconversion between structural intermediates that define kinetic states of their gating cycle (1–4). Such structural changes regulate the selective flow of K^+ ions down their electrochemical gradient and by extension, control the cell membrane potential (5). Two different structural motifs within the channel's PD, the activation gate (AG) and the selectivity filter (SF) (Fig. 1*A*), are functionally and structurally coupled (AG ⇔ SF coupling) in the sense that opening of the former triggers structural changes of the latter (by allosteric coupling). In a physiological context, the opening of a K^+ channel's AG initially allows the rapid and selective electrodiffusion of K^+ out of the cell and then causes a structural distortion of the channel's SF, leading to its structural collapse (i.e., a deep C-type inactivated state) (1, 2, 6–8) (Fig. 1*B*). Finally, it was suggested that, in KcsA, the opening of the AG triggers the transition of the SF from a "prime-to-conduct" conformation to a short-lived conductive one before undergoing C-type inactivation gating (9).

Previously, an allosteric hot spot for the AG ⇔ SF coupling in the PD of KcsA and *Shaker* channels was identified by functional, crystallographic, and computational approaches (Fig. 1*C*). In this study, Phe-103 and Ile-470 located on the pore-lining helices of the archetypal KcsA and Shaker channels, respectively, were shown to be critical components of the AG ⇔ SF coupling (1, 7, 10, 11), an observation independently corroborated by others (6, 8, 12–14) (Fig. 1 *B* and *C*).

In KcsA, Phe-103 is energetically coupled to several amino acid residues on the C-terminal end of the pore helix, among them Thr-75 (1, 2, 7) (Fig. 1*C*), a highly conserved residue within the signature sequence of K^+ channels (TTVGYGD) (15), which henceforth will be referred to as the second Threonine (Fig. 1*D*).

Results

Modifying AG ⇔ SF Allosteric Coupling in K^+ Channels. We tested the hypothesis that the second Threonine is an essential component of the allosteric network that mediates the AG ⇔ SF coupling, which is associated with C-type inactivation in KcsA as well as in the prototypical *Shaker* channel and its human homolog the hKv1.5 delayed rectifier voltage-gated channel. To this end, a unique multipronged approach was applied, which involved modifying the AG ⇔ SF coupling by introducing a perturbation by site-directed mutagenesis at the second Threonine. This was followed by a systematic evaluation at the functional level by electrophysiology and at the structural level by X-ray crystallography in a state-dependent manner (i.e., in the closed and open states of KcsA).

We reasoned that the simplest perturbation that could modify KcsA's AG ⇔ SF coupling without compromising protein folding was to substitute the second Threonine with an Alanine residue (T-to-A) at position 75. The T75A mutant abolished KcsA C-type inactivation as a consequence of perturbing the channel's AG ⇔ SF coupling (Fig. 1*E*) ($n = 10$). In addition, this mutant, after activating, displayed a time-dependent increase in current amplitude (Fig. 1*E*) ($n = 10$) and an ∼17 drop of the single-channel conductance (Fig. 1 *F–I*) [chord conductance at 100 mV, WT KcsA = 120 ± 7 pS ($n = 6$) and T75A = 7.1 ± 1 pS ($n = 5$)].

Significance

In K^+ channels, an allosteric coupling between their activation gate and selectivity filter underlies C-type inactivation coupled to activation gating. We have found that the second Threonine within the TTVGYGD signature sequence of K^+ channels is a crucial player for this allosteric communication. Interestingly, an Alanine substitution at this position in K^+ channels from bacteria to humans removed C-type inactivation gating and strikingly inverted the allosteric coupling (i.e., closing of the activation gate collapses the channel's selectivity filter, closed-state inactivation gating). Finally, we provide a crystallographic demonstration that closed-state inactivation can be achieved by the structural collapse of the channel's selectivity filter.

Author contributions: A.J.L. and L.G.C. designed research; A.J.L., D.M.C., C.T., and L.G.C. performed research; D.M.C. and C.T. contributed new reagents/analytic tools; A.J.L., D.M.C., and L.G.C. analyzed data; and A.J.L. and L.G.C. wrote the paper.

The authors declare no conflict of interest.

This article is a PNAS Direct Submission.

Data deposition: The crystallography, atomic coordinates, and structure factors have been deposited in the Protein Data Bank, www.wwpdb.org (PDB ID codes 6BY2 and 6BY3).

[1]Present address: Department of Antibody Engineering, Genentech, Inc., South San Francisco, CA 94080.

[2]To whom correspondence should be addressed. Email: luis.cuello@ttuhsc.edu.

This article contains supporting information online at www.pnas.org/lookup/suppl/doi:10.1073/pnas.1800559115/-/DCSupplemental.

Published online May 7, 2018.

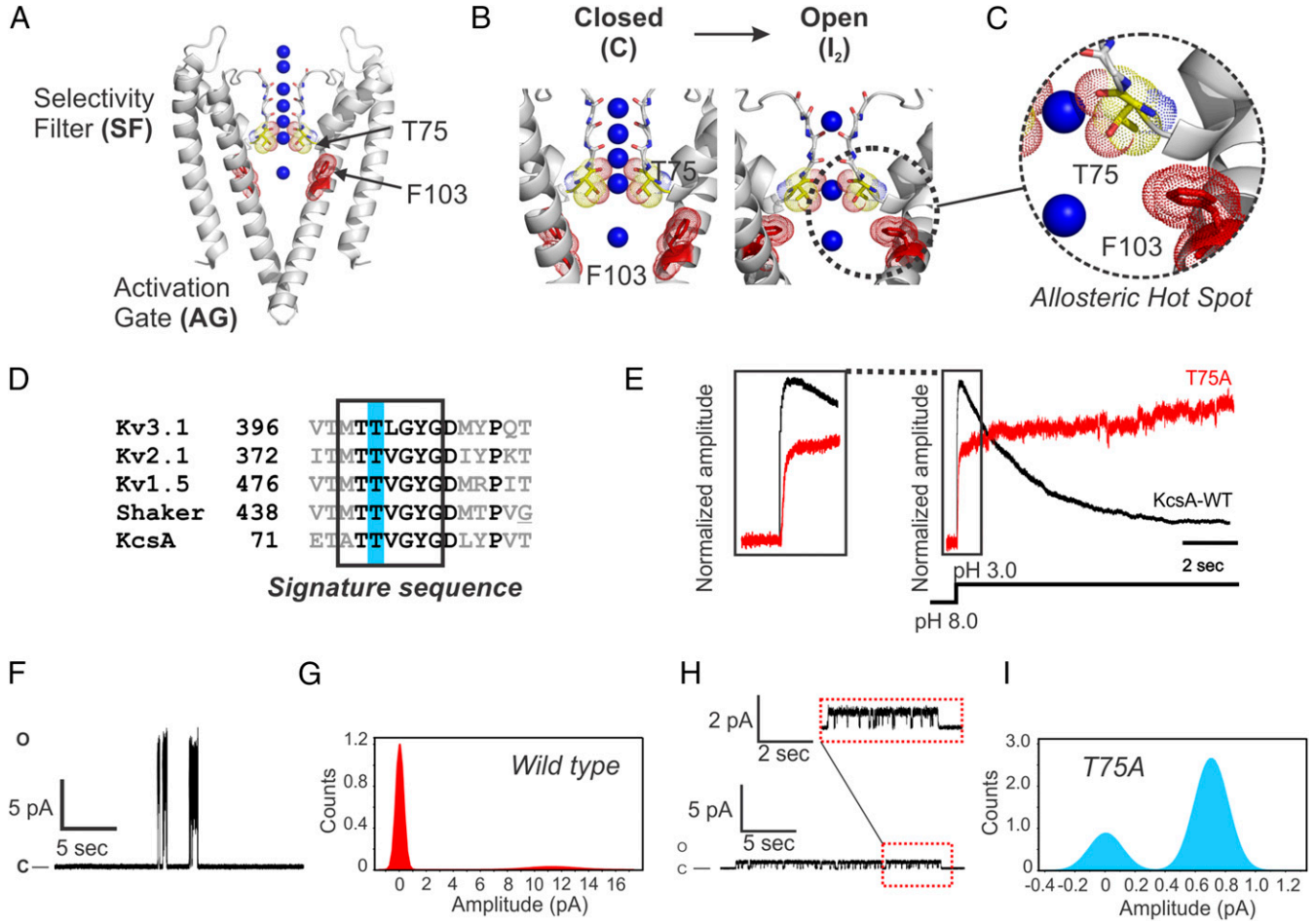

Fig. 1. (*A*) An "allosteric hot spot" in KcsA. Cartoon representation of closed KcsA (PDB ID code 1K4C) highlighting the channel's SF and AG. At the center of KcsA, F103 and T75 are shown (second Threonine within the signature sequence of K^+ channels) in dot representation. (*B*) On intracellular acidification, KcsA's AG opens and due to an allosteric communication, distorts the channel's SF, eventually driving it to a deep inactivated state or structurally collapsed I_2 (*Left*; a filter containing four bound K^+ ions). (*C*) A magnified view of KcsA's allosteric hot spot for inactivation coupled to activation gating showing F103 and T75 as putative interacting residues. (*D*) A sequence alignment between representative members of the delayed rectifier voltage-gated K^+-channel family and KcsA underscoring the high sequence identity of the K^+ signature sequence and the relative position of the second Threonine within it. (*E*) Amplitude normalized macroscopic currents for the WT KcsA (black trace) and the T75A mutant (red trace) channels recorded in symmetric 200 mM KCl during pH fast-switching experiments ($n = 10$; KcsA WT and T75A mutant were reconstituted in 1:20 and 1:100 protein to lipid ratios, respectively). *Left* shows the kinetics of activation for both WT KcsA and T75A mutant channels. (*F* and *H*) Representative steady-state, single-channel activity was measured in 200 mM KCl (pH 4.0) at 100 mV for WT KcsA ($n = 6$) and T75A mutant channels ($n = 5$). *H*, *Upper* shows a magnification of the T75A single-channel recording. (*G* and *I*) Chord conductance at 100 mV for WT KcsA of ~120 ± 7 pS and for T75A of ~7.1 ± 1 pS was calculated from Gaussian fits to closed and open event distributions in all points histograms. KcsA WT and the T75A mutant channels displayed nominal NPo (number of channels × open probability) of ~0.18 and 0.73, respectively.

Given the high degree of structural conservation at the PD of the Kv-channel family (16) and the bacterial K^+ channel KcsA (17, 18), we reasoned that a T-to-A mutation at the second Threonine of delayed rectifiers Kv channels (Fig. 1*D*) should alter the channel's AG ⇔ SF coupling in the same manner.

In the human delayed rectifier hKv1.5 and the *Shaker* channels, prolonged depolarization induces a time-dependent reduction of the macroscopic current amplitude due to the developing of C-type inactivation (19, 20). A conditioning test pulse to 0 or −80 mV allowed us to quantify the decrease in current amplitude by measuring the currents elicited by a subsequent test pulse to +60 mV. A reduction in current amplitudes (C-type inactivation) for these two Kv channels of about ~50–80% was observed ($n = 5$) (Fig. 2).

In contrast, a T-to-A mutation at the second Threonine of this subset of delayed rectifier Kv channels did not display the typical time-dependent reduction of current amplitude as if C-type inactivation has been removed. Paradoxically, the mutant channels displayed an increase in the current amplitudes elicited by a +60-mV test pulse after the conditioning pulse (Fig. 2). The T-to-A mutation was well-tolerated, yielding WT-like voltage-dependent channels (*SI Appendix*, Fig. S1)

The activation of the hKv1.5 T-to-A mutant macroscopic currents was biphasic, with a highly voltage-dependent fast component and a virtually voltage-independent slow component. We hypothesized that the second slow component of these mutants could be the manifestation of structural changes similar to C-type inactivation given that the kinetics of both processes are virtually voltage independent (*SI Appendix*, Fig. S2). Intriguingly, the kinetics of the T-to-A mutants activation and of the WT channel C-type inactivation are very similar (Fig. 2), which can be interpreted as if an inversion of the AG ⇔ SF coupling had occurred. Regardless of the dramatic changes in gating behavior, the T-to-A mutant channels remained highly K^+ selective (*SI Appendix*, Fig. S3 and Table S1).

A K^+ Channel Mutant with Inverted Allosteric Coupling. A possible explanation for the increase in current amplitude in the T-to-A

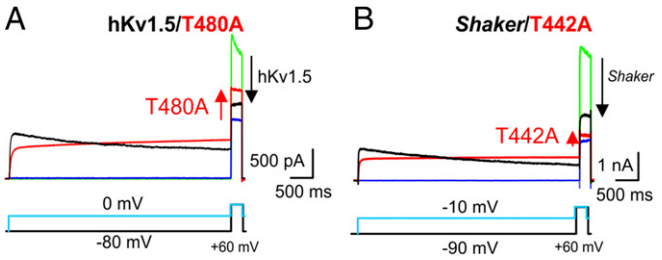

Fig. 2. Effect of prolonged depolarization on the current amplitude of delayed rectifier Kv channels. (*A* and *B*) Representative macroscopic current recordings for WT hKv1.5 (*A*) and *Shaker* (*B*) channels (black traces indicate pulse to 0 mV, and green traces indicate pulse to −80 mV) and their Alanine for Threonine substitution at the second Threonine of the K^+-channel signature sequence (red traces indicate pulse to −10 mV, and blue traces indicate pulse to −90 mV). Current recordings were elicited with pulse protocols shown below. The zero-current level is indicated by the horizontal bar at the beginning of the recording. (*A*) A prolonged depolarization (pulse to 0 mV) induces C-type inactivation in WT hKv1.5, which manifests as a time-dependent reduction in current amplitude (black trace; $n = 5$). This decrease in current amplitude can be quantified by comparing the current elicited by a test pulse at +60 mV after a conditioning test pulse to 0 mV (black) or to −80 mV (green); the magnitude of the current reduction is proportional to the size of the arrow at the end of the recording. For the mutant T480A, the current amplitude slowly increased during membrane depolarization. Note the increase in current amplitude (red arrow) during the +60-mV test pulse between a conditioning prepulse to −80 mV (blue) or 0 mV (red). (*B*) Due to the C-type inactivation process, the current of WT *Shaker* channels, alike to hKv1.5, decreased in a time-dependent fashion on prolonged depolarization (black traces; $n = 5$). In contrast, the second Threonine to Alanine mutant Shaker-T442A did not undergo C-type inactivation (red) and similar to hKv1.5-T480A and KcsA-T75A (Fig. 1*E*), displayed a time-dependent increase in current amplitude during prolonged activation ($n = 5$).

mutants is that their SF converts from a C-type inactivated state to a conductive and noninactivating conformation on AG opening. To test this idea, we used the hKv1.5-T480A mutant and applied the following pulse protocol. We applied a test pulse to +60 mV for 5 s (which elicited a noninactivating, biphasic macroscopic current with a fast increase in current amplitude followed by a slower one) (black trace in Fig. 3*A*) and then a 15-s repolarizing pulse to close the channels' AG. On a subsequent second test pulse to +60 mV (red trace in Fig. 3*A*), the amplitude of the fast component was increased and equaled the final amplitude of the first current trace (Fig. 3*A*) ($n = 5$).

Prolonging the interpulse duration at −80 mV from 2 to 600 s reversed the hKv1.5-T480A mutant current amplitude back to its initial value (Fig. 3 *A* and *B*). This strongly suggested the presence of a use-dependent conversion of the channel SF from a nonconductive to a conductive conformation and vice versa: a conversion that is associated with the channel's activation gating. The reversion of the SF to its nonconductive conformation was essentially voltage independent (Fig. 3*C*) ($n = 5$), which further suggests that the slow increase in current amplitude on prolonged depolarization presented by the T-to-A mutant channels is likely caused by structural changes similar or related to C-type inactivation.

If the slow increase in current amplitude displayed by T-to-A mutant channels is caused by the conversion of their SF from a C-type inactivated to a conductive conformation, then it should depend on the external K^+ concentration [K^+_o] (a hallmark of the C-type inactivation mechanism). We tested this possibility using a pressurized fast perfusion system and titrating the [K^+_o] in a stepwise fashion from 4 to 148 mM and measured the current amplitude elicited by a prolonged depolarization. In the hKv1.5 WT channel, the increase of the [K^+_o] produced the expected reduction of the current amplitude due to the decrease of K^+ chemical gradient (Fig. 4*A*). In contrast, the hKv1.5-T480A mutant displayed a robust increment in current amplitude, despite the decrease of the K^+ chemical gradient (Fig. 4*B* and *SI Appendix*, Fig. S4). The dependence of the current amplitude on the [K^+_o] displayed by the hKv1.5-T480A channels strongly suggests that this process is related to C-type inactivation gating. In other words, we hypothesize that most of the T480A channels are inactivated in their closed state (a collapsed SF in the closed state); then, augmenting the [K^+_o] biases the conformation of the T480A's SF to the conductive conformation, which causes the observed increase in current amplitude. To provide further support to the notion of closed-state inactivation in the hKv1.5-T480A mutant, we decided to study the effect of Rb^+ on the T480A increase in current amplitude on prolonged depolarization given its well-known effect relieving C-type inactivation in K^+ channels (10, 19, 21). *SI Appendix*, Fig. S5 shows a statistically significant 3–5% reduction of the hKV1.5 WT C-type inactivation rate. Based on this result, we reasoned that an increase in the [Rb^+_o] should relieve the T480A closed-state inactivation; hence, the augmentation in current amplitude

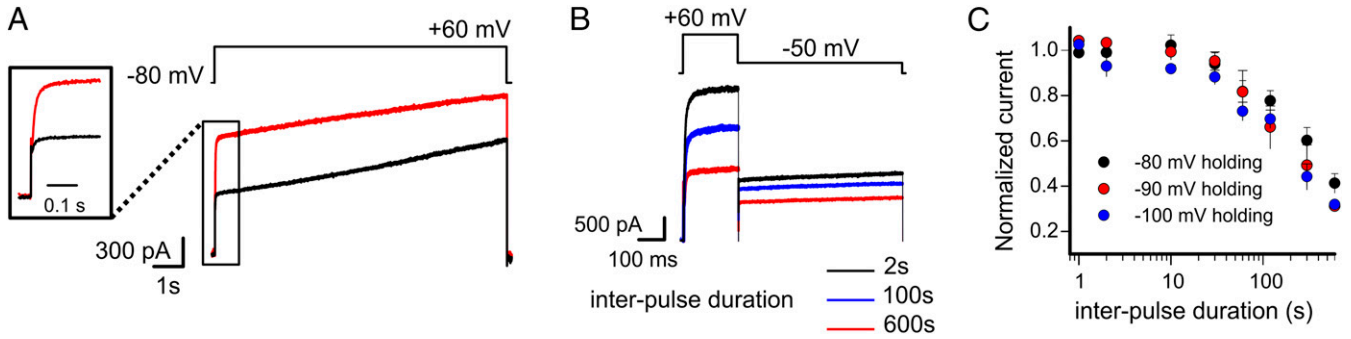

Fig. 3. Prolonged membrane depolarization recruits hKv1.5-T480A channels to their conducting states. (*A*) During the first 5 s of a depolarization test pulse to +60 mV (pulse protocol shown in *Upper Right*), there is a gradual increase in current amplitude (black trace); 15 s later, a second test pulse to +60 mV elicited a current (red trace), in which the amplitude of the fast component at the start of the depolarization test pulse is larger and equaled the final amplitude of the first macroscopic current (black trace). *Left* shows a magnified view of the first 200 ms, showing that the second macroscopic current (red trace) did not show an instantaneous current. This indicates that the hKv1.5-T480A mutant closed completely its AG during the 15 s at −90-mV holding potential ($n = 5$). (*B*) Increasing the interpulse duration from 2 s (black trace) to 100 s (blue trace) or 600 s (red trace) reverted the hKv1.5-T480A current amplitude at the beginning of the test pulse back to its initial values (i.e., the current amplitude of the fast component decreases; $n = 5$). (*C*) Normalized current amplitude of the fast component as a function of interpulse repolarization time at holding potentials of −80 mV (black), −90 mV (red), and −100 mV (blue; $n = 5$).

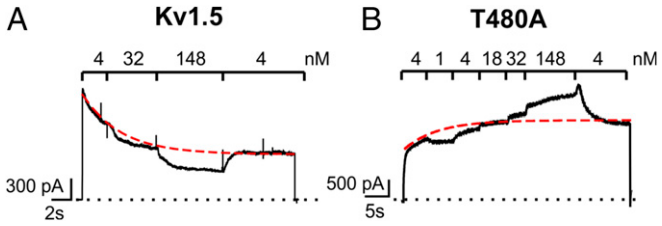

Fig. 4. Increased external [K^+] drive hKv1.5-T480A channels to their conducting states. Using a pressurized fast perfusion system, the external K^+ concentration was changed during a prolonged depolarization to +40 mV. (*A*) A representative macroscopic current of WT hKv1.5 showing the effects on the current amplitude of stepwise increases in external K^+ concentration. The red dashed line represents the expected current amplitude with a 4 mM extracellular K^+ concentration (the decrease is due to channel C-type inactivation). Increasing the external K^+ concentration (i.e., to 148 mM) at +40 mV lowers the electrochemical driving force for K^+ and results in a smaller outward current (n = 5). (*B*) A hKv1.5-T480A macroscopic current showing the effect of increasing the external K^+ concentration. In contrast to the result in WT hKv1.5, elevating the external K^+ concentration increased T480A current amplitude, despite the reduced outward electrochemical driving force for K^+. Switching back the extracellular K^+ concentration to 4 mM at the end of the recording resulted in a transient increase in current amplitude (in agreement with a stronger outward electrochemical driving force) followed by current decrease. The red dashed line represents the expected current amplitude when the extracellular solution contains 4 mM K^+ (n = 5).

should be more evident. *SI Appendix*, Fig. S6*A* shows that an increase of the [Rb^+_o] (5–10 mM), as predicted, triggered a more pronounced surge of the current amplitude, which is dependent on the [Rb^+_o]. In *SI Appendix*, Fig. S6*B*, it is shown that increasing the [Rb^+_o] to 10 mM produced a 2.7-fold increase of the T480A steady-state current on activation at +50 mV (n = 5), which strongly suggests that extracellular rubidium has biased the channel's SF conformation from a C-type inactivated to a conductive one.

Altogether, these results strongly suggest that substituting the second Threonine within the signature sequence of K^+ channels with an Alanine triggered the inactivation of the channel's SF in the closed state. It follows that the T-to-A mutants seem to invert the allosteric coupling between AG and SF in this subset of K^+ channels that undergo C-type inactivation gating. That is to say, the SF is inactive in the closed state and becomes conductive and noninactivating in the open state.

An important condition to show that the T-to-A mutant channels have an inverted AG ⇔ SF coupling is that their AG must display a normal gating process. A close inspection of the macroscopic currents deactivation of the T-to-A mutants indicated that their AG closes completely, albeit displaying slower kinetics (*SI Appendix*, Fig. S1). Fig. 3*A* clearly showed that a 15-s interpulse time was more than sufficient to totally shut the hKv1.5-T480A's AG.

Additionally, we directly tracked the pH-dependent conformational changes of KcsA's AG by continuous-wave EPR (CW-EPR) spectroscopy and site-directed spin label at the position G116, which is located at the channel's AG. The KcsA-T75A's AG on intracellular acidification undergoes conformational changes that are indistinguishable from those displayed by the WT channel (*SI Appendix*, Fig. S7). Interestingly, the pK_a of activation and the pK_a of deactivation of the T75A mutant were identical as has been evidenced in other noninactivating mutants of KcsA. In KcsA WT, the opening and closing of the AG display a hysteretic behavior, which is absent when C-type inactivation gating is removed (22). This result indicates that a T-to-A mutation causes the inversion of the AG ⇔ SF coupling in K^+ channels that undergo C-type inactivation. Collectively, our data unambiguously show that the AG can close independent of the SF's status and provide strong support for the proposed four-state kinetic model for KcsA gating (1).

A Crystallographic Demonstration of KcsA's Allosteric Coupling Inversion. To determine the structural changes that regulate the functioning of a K^+ channel, it is necessary to trap the channel's conformation as it changes along its gating cycle and solve the structures of these kinetic intermediates at atomic resolution. Previously, we have reported the generation of a disulfide-bridged locked open state for the KcsA channel (locked open KcsA) that allowed us to solve the structures of KcsA's open gating intermediates (1).

Given the functional equivalence between bacterial (KcsA), fruit fly (*Shaker*), and human (hKv1.5) potassium channels shown in this work, we pursued the structural basis of the functional effects of the T-to-A mutation by crystallizing and obtaining the X-ray crystal structures of the KcsA-T75A mutant in the closed and open states.

The structure of the closed KcsA-T75A mutant [T75A-closed; Protein Data Bank (PDB) ID code 6BY2] diffracted X-rays to 2.4-Å Bragg spacing. The structure was solved by molecular replacement, and the final refined model retained appropriate stereochemistry: R_{work} = 0.22 and R_{free} = 0.24 (*SI Appendix*, Table S2). The T75A-closed structure represents the atomic description of closed-state inactivation in a K^+ channel and provides a structural snapshot at an unknown kinetic intermediate within the KcsA gating cycle: the closed and deep C-type inactivated conformation (closed inactive state) (1). The T75A's AG, which is normally the narrowest region of the permeation pathway (~4 Å in diameter), is tightly closed, precluding the flow of K^+ ions across the channel. This is in total agreement with our CW-EPR measurements that indicated a closed AG at basic pH.

Previously, it has been shown that the structures of the closed KcsA in high-K^+ concentration (PDB ID code 1K4C) (23) and of the open noninactivating mutant (E71A) (1) reveal four K^+ bound to the SF, which correspond to the overlap of two isoenergetic ion configurations within the crystal lattice: S1–S3 and S2–S4, respectively (24).

The structure of the T75A-closed structure, although solved in the presence of 300 mM [K^+], contains only two K^+ ions, which are bound to positions S1 and S4 (the K^+ bound to the fourth binding site is exclusively coordinated by the alanine 75 main-chain carbonyl groups) (Fig. 5*A*). In addition, the T75A-closed structure shows an SF collapsed or deep C-type inactivated (mostly due to a 2-Å constriction at the level of Gly-77) (Fig. 5*B*). The T75A-closed structure SF is similar to the one found in the low-K^+ concentration (PDB ID code 1K4D) (23) and in KcsA with the AG open and an SF in a deep C-type inactivated conformation (1, 2). A structural alignment of the T75A-closed state (PDB ID code 6BY2) and the KcsA low-[K^+] (PDB ID code 1K4D) SF shows that they are essentially identical: rmsd 0.22 Å (Fig. 5*C*). The most remarkable difference is ~2-Å reduction of the interatomic distance between the K^+ bound at the S1 and S4 ion binding sites of the T75A SF-closed structure (Fig. 5*C*).

Crystallization trials using the locked open KcsA mutant with the T-to-A mutation at position 75 (T75A-open; PDB ID code 6BY3) yielded crystals in the I4 space group that diffracted X-rays at ~2.4 Å. A structural model was generated by molecular replacement and refined until obtaining adequate R_{work} and R_{free} of 0.20 and 0.22, respectively. The AG of the T75A-open structure spans about ~24 Å, which is about five times the size of a hydrated K^+ ion, and hence, it should allow free diffusion down its electrochemical gradient.

The functional analysis of the T-to-A mutants revealed fully K^+-selective (*SI Appendix*, Table S1) noninactivating channels. These experimental results strongly suggest that the second

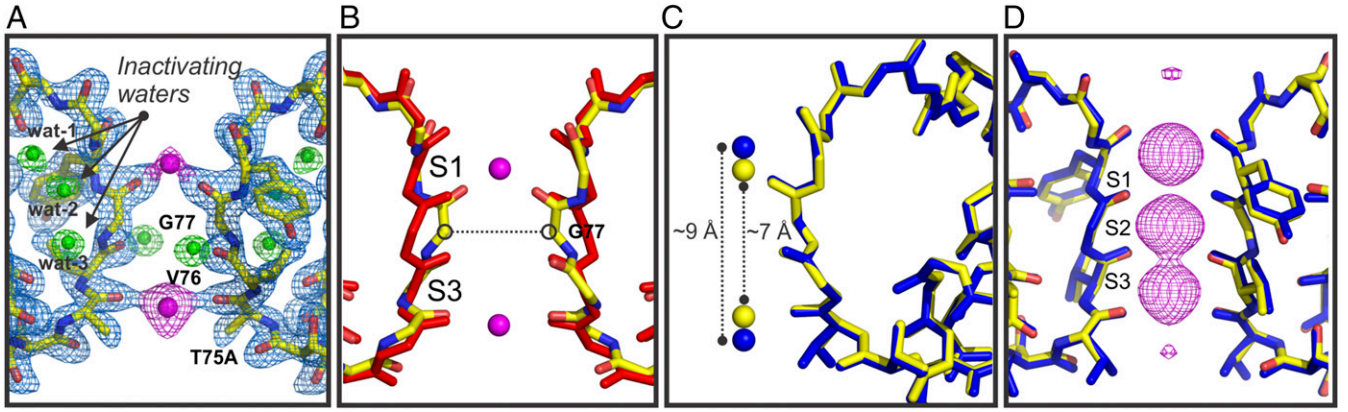

Fig. 5. Crystal structures of KcsA-T75A in the closed and open conformations. (*A*) The SF of the closed T75A mutant showing only two subunits for simplicity. The 2Fo-Fc electron density map is shown in light blue mesh (contoured at 2σ) for the channel's SF and in magenta (contoured at 4σ) for the two K^+ bound to the SF. Behind the SF, three water molecules in green (contoured at 3σ) are tightly bound between them by hydrogen bonds. Wat-3 is hydrogen bonded with the carbonyl group of Val-76 from a neighboring subunit, and this interaction keeps this carbonyl group in a flipped configuration incapable of binding K^+ ions. The structure of the T75A in its closed state represents a closed deep C-type inactivated state of KcsA. (*B*) Structural alignments of WT KcsA (PDB ID code 1K4C; red sticks) and the closed T75A mutant (PDB ID code 6BY2; yellow sticks) SF show a clear constriction at G77. (*C*) A structural alignment overlapping the SFs of the low-[K^+] (blue) and T75A-closed (yellow) structures. The rmsd of the two filter structures is 0.21 Å. The K^+ bound at the first and fourth binding sites gets closer (~2 Å) in the T75A-closed structure. (*D*) Structural alignment of the open conductive and noninactivating KcsA-E71A (blue sticks; PDB ID code 5VK6) and T75A-open (yellow sticks; PDB ID code 6BY3) mutants SFs shows no discernible differences between them. They are essentially identical. The atomic deviation between the two SFs peptide backbones (rmsd) is 0.25 Å. A mesh representation of a 2Fo-Fc electron density map (contoured at 3σ) validates the occupancy of three K^+ within SF at positions 1–3 with significantly reduced occupancy or no occupancy at position 4.

Threonine is an essential component of the allosteric network that communicates the AG and the SF in K^+ channels, since by replacing it, we surgically removed C-type inactivation gating (inactivation from the open state). The KcsA T75A-open structure displayed two very important features of a non–C-type inactivating K^+ channel: first, an SF displaying no detectable constriction at the level of Gly-77 and second, the presence of at least three consecutive K^+ bound to the channel's SF (we proposed that two consecutive ion vacancies within a K^+ channel's SF represent an insurmountable energetic barrier for ion permeation) (2) (Fig. 5*C*).

An SF with a suboptimal three K^+-bound configuration produced a profound impact in the turnover rate of K^+ transport for all of the T-to-A mutants studied here as was evidenced in a 2- to 17-fold drop in the mutant channel's unitary conductance (Fig. 1 *H* and *I* and *SI Appendix*, Table S1). However, all T-to-A mutants remained highly K^+ selective, albeit having only three K^+ bound to their SF. These experimental findings argue against the idea that high ion selectivity in K^+ channels is only possible in the presence of the canonical four K^+-bound configuration as previously proposed (25).

Discussion

In potassium channels, an allosteric coupling between their AG and SF is responsible for C-type inactivation coupled to activation gating (i.e., opening of the AG triggers the collapse of the channel's SF) (7, 8, 10, 11, 26). We have identified the second Threonine residue within the TTVGYGD signature sequence of K^+ channels as a crucial residue for this allosteric communication. A T-to-A mutation at this position produces an inversion of this allosteric mechanism in three representative members of the K^+-channel family. Fig. 6 shows a four-state kinetic model for KcsA's gating cycle as it has been described before (1). It illustrates an alternative path that is likely transited by the T-to-A mutant in KcsA, hKv1.5, and the *Shaker* channel when undergoing activation gating (Fig. 6, blue arrows). A T-to-A mutation at the second Threonine of the signature sequence of K^+ channels is inactive in the closed state, and during activation gating, their SF slowly transitions from a deep inactivated conformation to a conductive (which is reflected in the increase in current amplitude on long depolarizations) and noninactivating state (as seen in macroscopic currents of the T-to-A mutant Kv channels reported in here and the structure of the T75A-open structure). Then, if the AG is closed for a very brief period of time, the

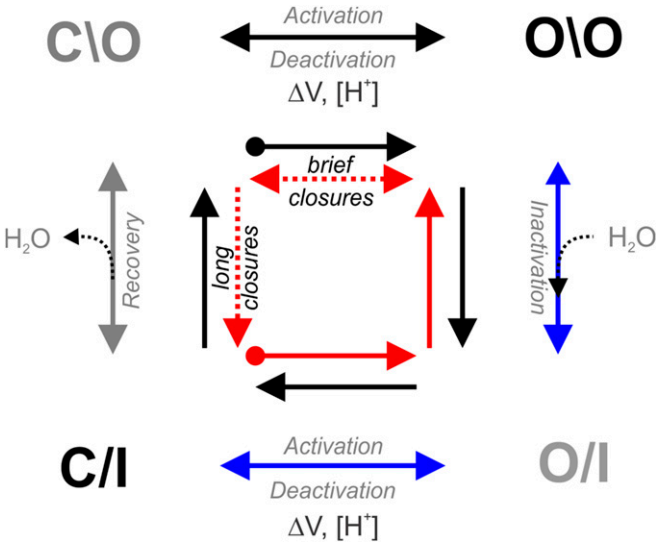

Fig. 6. A four-state kinetic cycle for the KcsA gating process. At neutral pH, KcsA-T75A mutant resides mostly in the closed inactive state (C/I); then, on intracellular acidification, the AG opens, but the SF remains inactive for a brief period of time [O/I (open and inactive)]. Due to an inversion of the allosteric coupling, the SF become conductive (blue arrows). Next, if the channel's AG is closed for a brief period of time (brief closures), the SF remains conductive (red arrows). Alternatively, when the T-to-A mutants are kept for longer times in the closed state (long closures), their SF initially remains conductive for a brief period of time and then undergoes C-type inactivation in the closed state (C/I; gray arrow), therefore resetting the system to the resting conformation. The circled end red and black arrows located at the center of the kinetic cycle indicate the starting kinetic states for KcsA WT (black) and the T75A mutant (red).

channel's SF remains conductive (Fig. 6, red arrows). Conversely, if the T-to-A mutants are kept in the closed state for longer periods (Fig. 3*B*), their SFs undergo C-type inactivation in the closed state (with their AG closed).

Together, based on functional and crystallographic evidence, it is clear that the T-to-A mutation in the subset of K^+ channels studied in this work not only uncoupled C-type inactivation from activation gating but also caused an inversion of the allosteric communication between the channel's AG and SF (i.e., AG closure triggers the SF collapse, and its opening does not cause C-type inactivation). Interestingly, a T-to-G mutation also induced the collapse of the SF in the closed state (27). Finally, our results provide structural snapshots that enrich the proposed four-state kinetic model for the PD of K^+ channels (1, 8) as well as the structure of the closed and C-type inactivated states of an ion channel (28–30).

Materials and Methods

Electrophysiological recordings for *Shaker*-IR and Shaker-IR-T442A [IR indicates fast inactivation removed (31)] were obtained from expression in HEK293 cells, since the Shaker construct expresses poorly in Ltk^- cells. External solutions with elevated K^+ concentration or 10 mM Rb^+ used to study the speed of selectivity filter conversion from its inactivated and collapsed state to its conducting open conformation as a function of external K^+ or Rb^+ concentration were obtained by replacing NaCl with KCl. Different external bath solutions were applied to the cells with a custom-built pressurized fast switching perfusion system (valves were purchased from the Lee Company) and a quartz micromanifold (ALA Scientific), allowing rapid exchange of the external bath solutions. Channels composed of the Alanine for Threonine substitution were recruited in their conducting configuration with repetitive depolarizations before applying the pulse protocol used for nonstationary noise analysis. For both WT and mutant channels, only cells that did not display current rundown during the train of repetitive depolarizations were used for analysis. Current recordings were analyzed using the built-in nonstationary fluctuation analysis tool of Pclamp10 software. This analysis tool calculates the ensemble current variance (σ^2) of the 100 tracings and plots it as a function of total current. KcsA T75A in the closed (32) or locked open scaffold [with KcsA activation locked open by disulfide bonds (1)] was transformed into *Escherichia coli*-XL10-Gold cells and grown overnight at 37 °C in LB media supplemented with 1% glucose and 0.4 mg/mL ampicillin (33). KcsA was extracted from *E. coli* membranes with Buffer A + 20 mM dodecyl maltoside (DDM) + protease inhibitors for 1 h at room temperature. The solubilized protein was separated from the insoluble material by spinning down at 100,000 × *g*. The supernatant was loaded onto a cobalt resin column, washed with Buffer A supplemented with 10 mM imidazole and 1 mM DDM, and eluted with Buffer A supplemented with 1 mM DDM and 400 mM imidazole. The analysis of KcsA properly folded was performed by size exclusion chromatography on an ENrich SEC 650 10 × 300 column (Bio-Rad). Crystal trials were set up by the sitting drop method in 24–27% (vol/vol) PEG 400, 50 mM magnesium acetate, and 50 mM sodium acetate (pH 5.4–6.0) at 19 °C. Crystals regularly appeared within a 2-wk period, and they were immediately cryoprotected. The structural models for the closed and open conformations of the T75A mutant were built from scratch using coot (34) and refined iteratively with Phenix (35), including rigid body, energy minimization, simulated annealing, and individual B-factor refinements. Additional details are described in *SI Appendix, SI Materials and Methods*.

ACKNOWLEDGMENTS. A.J.L. thanks E. Mayeur for continued support. L.G.C. thanks Luis Gonzalo Cuello Fumero and Aminta Apolonia Cuello for their constant support and Dr. Luis Reuss for his continuous technical advice and proofreading the manuscript. We thank the members of the L.G.C. laboratory for technical advice on this project. We thank Silvia Russi at the Stanford Synchrotron Radiation Laboratory Beamline 14-1. Dr. Roderick Mackinnon generously provided the hybridoma cells for Fab production. This work was supported in part by a Center for Membrane Protein Research-Texas Tech University Health Sciences Center Seed Grant, American Heart Association Grant 11SDG5440003, National Institutes of Health Grant 1RO1GM097159-01A1, and Welch Foundation Grant BI-1757.

1. Cuello LG, Cortes DM, Perozo E (2017) The gating cycle of a K^+ channel at atomic resolution. *eLife* 6:e28032.
2. Cuello LG, Jogini V, Cortes DM, Perozo E (2010) Structural mechanism of C-type inactivation in K(+) channels. *Nature* 466:203–208.
3. Liu Y, Jurman ME, Yellen G (1996) Dynamic rearrangement of the outer mouth of a K+ channel during gating. *Neuron* 16:859–867.
4. Loots E, Isacoff EY (1998) Protein rearrangements underlying slow inactivation of the Shaker K+ channel. *J Gen Physiol* 112:377–389.
5. Hille B (1992) *Ionic Channels of Excitable Membranes* (Sinauer, Sunderland, MA), 2nd Ed.
6. Ben-Abu Y, Zhou Y, Zilberberg N, Yifrach O (2009) Inverse coupling in leak and voltage-activated K+ channel gates underlies distinct roles in electrical signaling. *Nat Struct Mol Biol* 16:71–79.
7. Pan AC, Cuello LG, Perozo E, Roux B (2011) Thermodynamic coupling between activation and inactivation gating in potassium channels revealed by free energy molecular dynamics simulations. *J Gen Physiol* 138:571–580.
8. Panyi G, Deutsch C (2006) Cross talk between activation and slow inactivation gates of Shaker potassium channels. *J Gen Physiol* 128:547–559.
9. Heer FT, Posson DJ, Wojtas-Niziurski W, Nimigean CM, Bernèche S (2017) Mechanism of activation at the selectivity filter of the KcsA K^+ channel. *eLife* 6:e25844.
10. Cuello LG, et al. (2010) Structural basis for the coupling between activation and inactivation gates in K(+) channels. *Nature* 466:272–275.
11. Peters CJ, Fedida D, Accili EA (2013) Allosteric coupling of the inner activation gate to the outer pore of a potassium channel. *Sci Rep* 3:3025.
12. Ader C, Pongs O, Becker S, Baldus M (2010) Protein dynamics detected in a membrane-embedded potassium channel using two-dimensional solid-state NMR spectroscopy. *Biochim Biophys Acta* 1798:286–290.
13. Sadovsky E, Yifrach O (2007) Principles underlying energetic coupling along an allosteric communication trajectory of a voltage-activated K+ channel. *Proc Natl Acad Sci USA* 104:19813–19818.
14. Wylie BJ, Bhate MP, McDermott AE (2014) Transmembrane allosteric coupling of the gates in a potassium channel. *Proc Natl Acad Sci USA* 111:185–190.
15. Heginbotham L, Lu Z, Abramson T, MacKinnon R (1994) Mutations in the K+ channel signature sequence. *Biophys J* 66:1061–1067.
16. Long SB, Campbell EB, Mackinnon R (2005) Crystal structure of a mammalian voltage-dependent Shaker family K+ channel. *Science* 309:897–903.
17. Doyle DA, et al. (1998) The structure of the potassium channel: Molecular basis of K+ conduction and selectivity. *Science* 280:69–77.
18. Morais-Cabral JH, Zhou Y, MacKinnon R (2001) Energetic optimization of ion conduction rate by the K+ selectivity filter. *Nature* 414:37–42.
19. Fedida D, Maruoka ND, Lin S (1999) Modulation of slow inactivation in human cardiac Kv1.5 channels by extra- and intracellular permeant cations. *J Physiol* 515:315–329.
20. Hoshi T, Zagotta WN, Aldrich RW (1991) Two types of inactivation in Shaker K+ channels: Effects of alterations in the carboxy-terminal region. *Neuron* 7:547–556.
21. López-Barneo J, Hoshi T, Heinemann SH, Aldrich RW (1993) Effects of external cations and mutations in the pore region on C-type inactivation of Shaker potassium channels. *Receptors Channels* 1:61–71.
22. Steeland S, Vandenbroucke RE, Libert C (2016) Nanobodies as therapeutics: Big opportunities for small antibodies. *Drug Discov Today* 21:1076–1113.
23. Zhou Y, Morais-Cabral JH, Kaufman A, MacKinnon R (2001) Chemistry of ion coordination and hydration revealed by a K+ channel-Fab complex at 2.0 A resolution. *Nature* 414:43–48.
24. Zhou M, Morais-Cabral JH, Mann S, MacKinnon R (2001) Potassium channel receptor site for the inactivation gate and quaternary amine inhibitors. *Nature* 411:657–661.
25. Derebe MG, et al. (2011) Tuning the ion selectivity of tetrameric cation channels by changing the number of ion binding sites. *Proc Natl Acad Sci USA* 108:598–602.
26. Ader C, et al. (2009) Coupling of activation and inactivation gate in a K+-channel: Potassium and ligand sensitivity. *EMBO J* 28:2825–2834.
27. Matulef K, Annen AW, Nix JC, Valiyaveetil FI (2016) Individual ion binding sites in the K(+) channel play distinct roles in C-type inactivation and in recovery from inactivation. *Structure* 24:750–761.
28. Aldrich RW (1981) Inactivation of voltage-gated delayed potassium current in molluscan neurons. A kinetic model. *Biophys J* 36:519–532.
29. Fineberg JD, Szanto TG, Panyi G, Covarrubias M (2016) Closed-state inactivation involving an internal gate in Kv4.1 channels modulates pore blockade by intracellular quaternary ammonium ions. *Sci Rep* 6:31131.
30. Yan J, Li Q, Aldrich RW (2016) Closed state-coupled C-type inactivation in BK channels. *Proc Natl Acad Sci USA* 113:6991–6996.
31. Hoshi T, Zagotta WN, Aldrich RW (1990) Biophysical and molecular mechanisms of Shaker potassium channel inactivation. *Science* 250:533–538.
32. Cortes DM, Perozo E (1997) Structural dynamics of the Streptomyces lividans K+ channel (SKC1): Oligomeric stoichiometry and stability. *Biochemistry* 36:10343–10352.
33. Tilegenova C, Vemulapally S, Cortes DM, Cuello LG (2016) An improved method for the cost-effective expression and purification of large quantities of KcsA. *Protein Expr Purif* 127:53–60.
34. Emsley P, Cowtan K (2004) Coot: Model-building tools for molecular graphics. *Acta Crystallogr D Biol Crystallogr* 60:2126–2132.
35. Adams PD, et al. (2010) PHENIX: A comprehensive Python-based system for macromolecular structure solution. *Acta Crystallogr D Biol Crystallogr* 66:213–221.